ChemComm

High Selectivity of CO2 Hydrogenation to CO by Controlling the Valence State of Nickel using Perovskite

Journal:	*ChemComm*
Manuscript ID	CC-COM-05-2018-003829.R1
Article Type:	Communication

ChemComm

COMMUNICATION

High Selectivity of CO_2 Hydrogenation to CO by Controlling the Valence State of Nickel using Perovskite

Received 00th January 20xx,
Accepted 00th January 20xx

DOI: 10.1039/x0xx00000x

www.rsc.org/

Baohuai Zhao,‡[ab] Binhang Yan,‡[bc] Zhao Jiang,[e] Siyu Yao,[b] Zongyuan Liu,[b] Qiyuan Wu,[d] Rui Ran,*[a] Sanjaya D. Senanayake,[b] Duan Weng[a] and Jingguang. G. Chen*[e]

The selectivity of CO_2 hydrogenation can be significantly tuned by controlling the valence state of nickel using lanthanum-iron-nickel perovskites. Nickel with higher valence states weakens the binding of CO and increases the activation barrier for further CO hydrogenation, leading to a higher CO selectivity than the metallic nickel.

Catalytic conversion of CO_2 has attracted increasing attention in recent years, aiming at alleviating the global warming and ocean acidification.[1-3] CO_2 hydrogenation with renewable hydrogen is proposed to utilize CO_2 as a raw material to produce valuable chemicals, such as CO, CH_4, and methanol. Ni-based catalysts are identified as one of the most promising catalysts for CO_2 hydrogenation due to their considerable catalytic activity and lower cost compared to precious metal catalysts.[4, 5] However, Ni-based catalysts are generally favorable for the Sabatier methanation reaction for CH_4 rather than the reverse water gas shift (RWGS) reaction for CO.[5, 6] In many cases, CO is more desirable than CH_4 as it offers more flexibility to produce oxygenates and synthetic fuels via the methanol synthesis or Fischer-Tropsch reactions.[7] Thus, it is important to promote the selectivity of CO_2 hydrogenation to CO over Ni-based catalysts.

To date, many attempts have been made to increase the CO selectivity over Ni-based catalysts, such as alloying Ni with other metals (Cu, Pt, and Pd et al.),[8, 9] controlling the loading of Ni,[10] and using promoters like K.[11] However, a fundamental understanding of the influence of the binding energies of the intermediates over Ni-based catalysts on the product selectivity is still lacking. In our previous studies, the correlation between the binding energies of key intermediates and the product selectivity for CO_2 hydrogenation was established through combined experiments and DFT calculations over several other catalysts.[7, 12-14] For example, by simply replacing the CeO_2 or ZrO_2 supports with TiO_2 for the PtCo-based bimetallic catalysts, the ratio of CO/CH_4 was increased since the binding of C,O-bound and O-bound species at the PtCo-oxide interface was weakened.[7] Although the mechanism of CO_2 hydrogenation is complicated and might be very different over various catalysts, it is generally accepted that CO is the key intermediate for CH_4 formation over Ni-based catalysts.[4, 11, 15, 16] This suggests that the product selectivity of CO_2 hydrogenation can be potentially tuned by controlling the binding energies of CO on the catalysts.

It is well known that the binding energy of CO varies with the valence state of nickel, which is much weaker on oxidized nickel than that on metallic nickel.[15] The weak binding energy of CO offers a potential way to promote the CO selectivity for CO_2 hydrogenation over Ni-based catalysts. However, for the supported Ni-based catalysts, nickel is more likely to be reduced to Ni^0 under hydrogenation conditions.[17] Therefore, keeping Ni at higher valence states under reaction conditions is a key challenge in promoting the CO selectivity. Perovskites with the ideal general formula of ABO_3 are known as versatile materials in which Ni ions can be located at the B sites. They could be reduced out of the perovskite lattice to form highly dispersed nanoparticles under particular environments, resulting in a strong metal support interaction (SMSI) effect.[18, 19] These features of Ni-containing perovskites were widely investigated and the related catalysts, such as $LaNiO_3$, $LaFe_{1-x}Ni_xO_3$, and $SrTi_{1-x}Ni_xO_3$, were used for many reactions including dry reforming or steam reforming of methane.[18, 20] Recently, Steiger et al. investigated the parameters for the regeneration behavior of the perovskite ($LaFe_{1-x}Ni_xO_3$) structure, using CO_2 hydrogenation as a probe reaction.[21] However, to the best of our knowledge, there are no discussions about controlling the selectivity of CO_2 hydrogenation using perovskites.

Herein, this study demonstrates how the selectivity of CO_2 hydrogenation can be tuned by changing the valence state of nickel using different lanthanum-iron-nickel perovskites. The catalytic performance using a flow reactor is shown in Fig. S1 and S2 (ESI†) and results obtained after the reaction reached a

[a] School of Materials Science and Engineering, Tsinghua University, Beijing 100084, China
Email: ranr@tsinghua.edu.cn
[b] Chemistry Department, Brookhaven National Laboratory, Upton, New York 11973, United States.
[c] Department of Chemical Engineering, Tsinghua University, Beijing 100084, China.
[d] Department of material Science and Chemical Engineering, Stony Brook University, Stony Brook, New York 11794, United States.
[e] Department of Chemical Engineering, Columbia University, New York, New York 10027, United States.
Email: jgchen@columbia.edu

† Electronic Supplementary Information (ESI) available: Experimental details, specific surface area, activity curves, H_2-TPR curves, additional XRD patterns, TEM figures, and XPS spectra. See DOI: 10.1039/x0xx00000x

‡ These authors contributed equally to this work.

steady-state at 14 hours at 673 K are summarized in Table 1. It is noticed that $LaNiO_3$ mainly produces CH_4 rather than CO while very little CH_4 is formed over $LaFe_{0.5}Ni_{0.5}O_3$. Table S1 (ESI†) compares the catalytic performance of a series of perovskites with different Fe/Ni ratios. $LaFeO_3$ shows poor activity with the lowest CO_2 and H_2 conversions. After doping Ni into the perovskites their activity is significantly increased, indicating that Ni-related species should be responsible for the production of CH_4 or CO over the Ni-containing perovskites. It is known that the selectivity of CO_2 hydrogenation over Ni-based catalysts often varies with CO_2 conversion, which depends on the gas space velocity and temperature. Here the CO_2 conversion of $LaNiO_3$ was controlled at a similar level with $LaFe_{0.5}Ni_{0.5}O_3$, i.e. 18.1%, and the selectivity is also listed in Table 1. It can be seen that even at similar CO_2 conversion $LaNiO_3$ still shows a much higher selectivity of CH_4 (71.4%) compared to $LaFe_{0.5}Ni_{0.5}O_3$ (3.2%).

Table 1: Summary of flow reactor data for CO_2 hydrogenation over $LaNiO_3$ and $LaFe_{0.5}Ni_{0.5}O_3$ (calculated by averaging data points in 12–14 h on stream, $CO_2/H_2/Ar$ = 5/10/25 mL min^{-1}).

Catalyst		$LaNiO_3$[a]	$LaFe_{0.5}Ni_{0.5}O_3$[a]	$LaNiO_3$[b]
Conversion (%)	CO_2	39.7	16.3	18.1
	H_2	75.5	11.4	28.4
TOF (mol mol_{Ni}^{-1} min^{-1})	CO_2	0.20	0.15	1.03
	H_2	0.75	0.21	3.19
Yield (%)	CO	3.2	15.8	5.1
	CH_4	36.5	0.5	12.9
Selectivity (%)	CO	8.0	96.6	28.2
	CH_4	92.0	3.2	71.4

[a] 100 mg catalyst, T = 673 K. [b] 15 mg catalyst, T = 623 K.

Fig. 1 shows the TEM images and particle size distributions of the spent catalysts. In Fig. 1a and d the Ni-related particles can be found on the surface of both spent catalysts, while no such particles are observed on the fresh catalysts (Fig. S3, ESI†), indicating that Ni ions were exsolved from the perovskite lattice to form surface nanoparticles. The magnified images in Fig. 1b and e reveal that the nanoparticles are closely attached to the perovskite host. The size distributions of the nanoparticles are shown in Fig. 1c and f. The average particle size in the spent $LaNiO_3$ and $LaFe_{0.5}Ni_{0.5}O_3$ are 6.5 and 4.5 nm, respectively. However, according to the general view of the catalysts derived from perovskites, the particles on the surface usually interact strongly with the support and their properties are significantly influenced by their parent lattice.[18, 21] Thus, the oxidation states of Ni in the nanoparticles are still unknown.

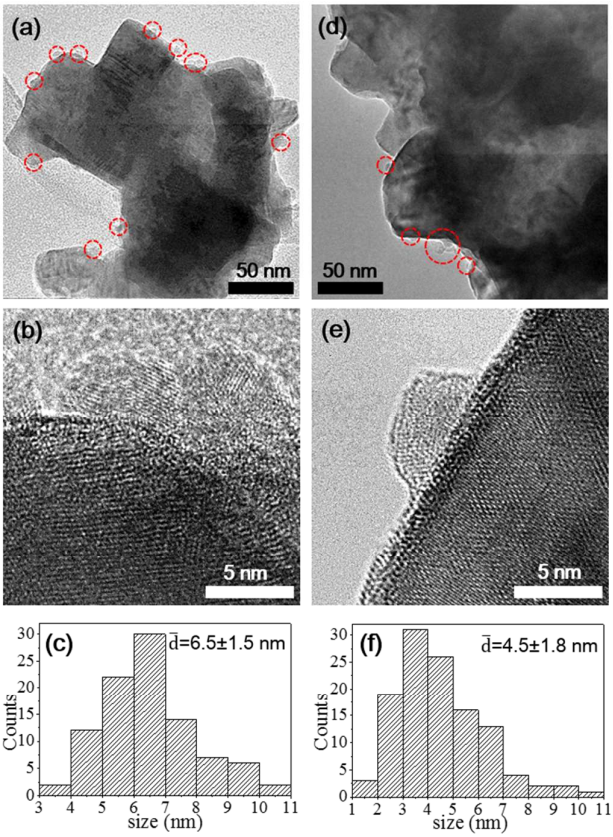

Fig. 1 TEM images and particle size distributions of the spent catalysts (a–c) $LaNiO_3$; (d–f) $LaFe_{0.5}Ni_{0.5}O_3$.

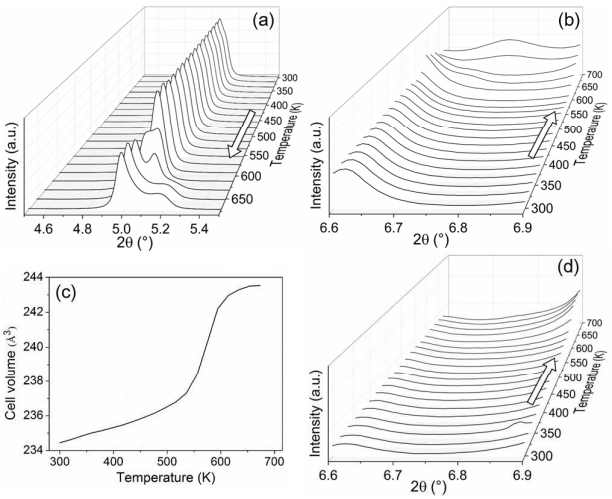

Fig. 2 Results of the *in-situ* XRD measurements during the temperature ramping stage, (a) and (b) patterns of $LaNiO_3$; (c) and (d) lattice expansion and patterns of $LaFe_{0.5}Ni_{0.5}O_3$. Fig. b and d show regions where Ni diffraction peaks would be expected.

To understand the structural evolution of the catalysts, *in-situ* XRD experiments for $LaNiO_3$ and $LaFe_{0.5}Ni_{0.5}O_3$ under reaction conditions were performed. Fig. 2a shows the strongest diffraction peak around 2θ = 5.0° of $LaNiO_3$ as a function of temperature from 300 to 673 K. It can be seen that the peaks start to slightly shift to lower angle position at 553 K

due to the exsolution of Ni ions and the phase transformation from $LaNiO_3$ to $LaNiO_{2.5}$ takes place at about 625 K. In Fig. 2b the diffraction peaks of metallic Ni centered at 2θ = 6.8° start to appear at 653 K, right after the phase transformation. These results suggest that a portion of the Ni ions in the $LaNiO_3$ perovskite is converted into metallic Ni under reaction conditions.[21] In the case of $LaFe_{0.5}Ni_{0.5}O_3$, its perovskite structure is still maintained after the reaction (Fig. S4, ESI†). In Fig. 2c there is an abrupt volume expansion occurred between 520 and 615 K on top of the upward-sloping background line from the thermal effect, demonstrating that there are Ni^{3+} ions coming out of the perovskite lattice.[19, 21] However, it should be noted that the diffraction peak of metallic Ni is almost invisible in the XRD patterns in Fig. 2d. The H_2-TPR results (Fig. S6, ESI†) are also consistent with that the $LaFe_{0.5}Ni_{0.5}O_3$ perovskite is able to stabilize Ni in the oxidized states until a higher temperature range than $LaNiO_3$. When changing the atmosphere to H_2+He at 673 K, the strongest diffraction peak in both catalysts are without further change (Fig. S5, ESI†), demonstrating that the changed structures are stable to endure such a reaction condition.

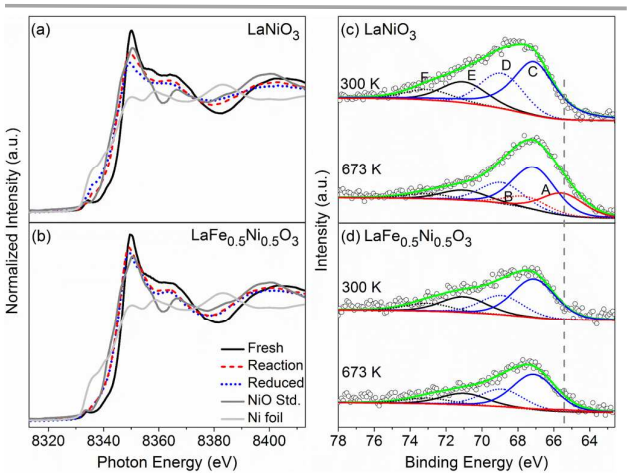

Fig. 3 *In-situ* XANES spectra of Ni K-edge of (a) $LaNiO_3$ and (b) $LaFe_{0.5}Ni_{0.5}O_3$. *In-situ* AP-XPS spectra of Ni 3*p* of (c) $LaNiO_3$ and (d) $LaFe_{0.5}Ni_{0.5}O_3$ at 300 K and 673 K, peak A and B correspond to the $3p_{3/2}$ and $3p_{1/2}$ of Ni^0, peak C and D correspond to the $3p_{3/2}$ and $3p_{1/2}$ of Ni^{2+}, peak E and F correspond to the $3p_{3/2}$ and $3p_{1/2}$ of Ni^{3+}.

In-situ X-ray absorption near-edge structure (XANES) measurements were performed to further understand the evolution of Ni ions in the perovskites. The XANES spectra of Ni K-edge for the two catalysts are shown in Fig. 3a and b. Ni in reduced oxidation states can be identified by the decreased white line in the spectra. The compositions are estimated by a linear combination fitting method and summarized in Table S2 (ESI†). The results indicate that metallic Ni exists (11%) in $LaNiO_3$ under reaction conditions, and its amount further increases to 41% when cutting off CO_2 in the stream. In contrast, the Ni-related species in $LaFe_{0.5}Ni_{0.5}O_3$ are almost without metallic Ni under both reaction and reduced conditions. As mentioned above, the Ni in supported catalyst is easy to be reduced to the metallic state. Here, a comparison between the Ni K-edge spectra of $LaFe_{0.5}Ni_{0.5}O_3$ and Ni/ZrO_2 under reaction condition is given in Fig. S7 (ESI†). It can be seen that $LaFe_{0.5}Ni_{0.5}O_3$ truly has the ability to maintain Ni in a higher valence state than the supported catalyst.

The aim of *in-situ* ambient pressure X-ray photoelectron spectroscopy (AP-XPS) experiments was to detect the oxidation states of surface Ni. They were carried out under 10 mTorr pressure of reactants (CO_2/H_2 = 1/2) and the Ni 3*p* spectra are adopted in this work since the Ni $2p_{3/2}$ and La $3d_{3/2}$ spectra strongly interfere with each other.[22] The Ni 3*p* spectra in Fig. 3c and d show changes in valence states between the catalyst at 300 K and during the reaction at 673 K. The spectra of $LaNiO_3$-300 K and $LaFe_{0.5}Ni_{0.5}O_3$-300 K show co-existence of Ni^{3+} and Ni^{2+}, with their $3p_{3/2}$ peaks appearing at approximately 70.9 and 67.0 eV, respectively.[22-25] The Ni^0 $3p_{3/2}$ peak as indicated by the dashed line (65.5 eV) is absent in both fresh catalysts.[25, 26] For the spectrum of $LaNiO_3$-673 K, the overall peak shifts to a lower binding energy range (Fig. S8, ESI†) due to a decrease in the intensity peaks assigned to Ni^{3+} and Ni^{2+}, together with the appearance of the Ni^0 peaks. In contrast, such a peak shift does not occur obviously between the two spectra of $LaFe_{0.5}Ni_{0.5}O_3$. The intensity of the peaks assigned to Ni^{3+} decreases in the spectrum of $LaFe_{0.5}Ni_{0.5}O_3$-673 K compared to that of $LaFe_{0.5}Ni_{0.5}O_3$-300 K. However, the peaks attributed to Ni^0 are very weak in $LaFe_{0.5}Ni_{0.5}O_3$-673 K. As summarized in Table S3 and S4 (ESI†), the peak area of Ni^0 in the spectrum of $LaNiO_3$-673 K accounts for 29.1% of the total peak area, while it is only 3.0% of the total peak area of $LaFe_{0.5}Ni_{0.5}O_3$-673 K. It should be noted that some metallic Ni might come from the Ni nanoparticles over the $LaFe_{0.5}Ni_{0.5}O_3$ surface. However, Ni in the nanoparticles of this sample should likely be in a mixed states of metallic Ni and Ni ions, as the nanoparticles strongly interact with the perovskite support[20] and the electronic properties of Ni in the nanoparticles should also be modified. Based on the *in-situ* XRD, XANES, and AP-XPS results, it is suggested that $LaFe_{0.5}Ni_{0.5}O_3$ is able to maintain the surface Ni species at a higher valence state in the reducing atmosphere.

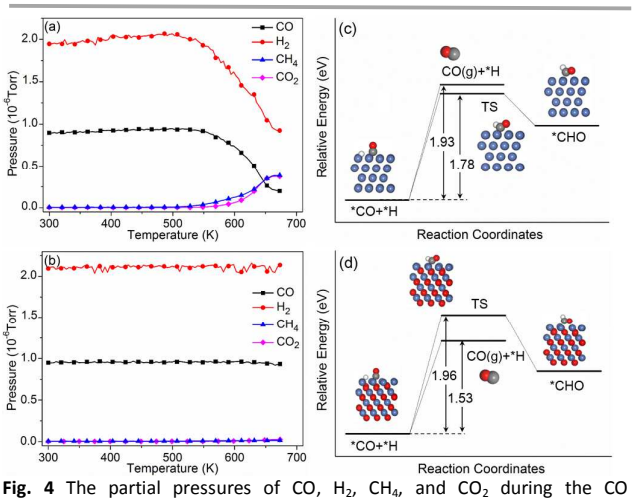

Fig. 4 The partial pressures of CO, H_2, CH_4, and CO_2 during the CO hydrogenation reaction for (a) $LaNiO_3$ and (b) $LaFe_{0.5}Ni_{0.5}O_3$. Potential energy diagram for the reaction routes of *CO+H on Ni(111) and NiO(111). The DFT optimized geometries of *H, *CO, transition states (TS), and *CHO on Ni(111) and NiO(111), are shown as insets in (c) and (d), Ni: blue, O: red, C: gray, H: white.

Density functional theory (DFT) calculations combined with the CO hydrogenation experiments were carried out to understand how

the valence states of Ni control the selectivity of CO_2 hydrogenation. Fig. 4a and b show the CO, H_2, CH_4, and CO_2 partial pressures during the CO+2H_2 reaction on $LaNiO_3$ and $LaFe_{0.5}Ni_{0.5}O_3$. $LaNiO_3$ is active for the further hydrogenation of the CO product; both CO and H_2 start to react at 525 K, and their pressures keep decreasing with a simultaneous increase in the CH_4 pressure. In contrast, $LaFe_{0.5}Ni_{0.5}O_3$ is inactive for CO hydrogenation in the entire temperature range. The results confirm that CO is a key intermediate for CO_2 hydrogenation to CH_4 and its reactivity is quite different over $LaNiO_3$ and $LaFe_{0.5}Ni_{0.5}O_3$.

DFT calculations were performed to correlate the binding energy of CO with the product selectivity by using Ni(111) and NiO(111) model surfaces simulating Ni oxidation states. According to previous studies, the RWGS + CO-Hydro pathway with key intermediates of CO and CHO is employed.[7, 11, 12, 27, 28] The optimized geometries and binding energies of CO and CHO species are shown in Fig. S9 and Table S5 (ESI†), respectively. According to the RWGS + CO-Hydro mechanism, the formed *CO either desorbs to produce gas phase CO or undergoes subsequent hydrogenation reaction to form CH_4. As shown in Fig. 4c the hydrogenation of *CO to *CHO on Ni(111) has an activation barrier (*E*a) of 1.78 eV, while the formation of CO should overcome a desorption energy (*E*d) of 1.93 eV, which is equal the BE of *CO on Ni(111). Such a strong binding makes the desorption of *CO difficult and thus it is more favorable for its further hydrogenation to *CHO and subsequently to CH_4. On the other hand, the hydrogenation of *CO to *CHO on NiO(111) has an *E*a of 1.96 eV, while the *E*d for CO is only 1.53 eV. Thus, the *CO desorption is more favorable than its hydrogenation to *CHO on the NiO(111) surface. Overall, the DFT calculations predict that the NiO(111) surface should be more selective than Ni(111) for CO production, consistent with the experimental results.

In conclusion, the combined *in-situ* experimental and theoretical investigations have shown that by changing the valence state of Ni, the product selectivity of CO_2 hydrogenation can be tuned over lanthanum-iron-nickel perovskites. $LaNiO_3$ shows high selectivity toward CH_4, whereas CO is preferentially formed on $LaFe_{0.5}Ni_{0.5}O_3$. According to the *in-situ* XRD, XANES, and AP-XPS analysis, metallic Ni is formed over $LaNiO_3$ under reaction conditions, while the Ni-related species present higher valence states in $LaFe_{0.5}Ni_{0.5}O_3$. DFT calculations reveal that CO binds weakly on NiO(111) where *CO desorption is more favorable over its further hydrogenation to CH_4, leading to a much higher CO selectivity. This correlates well with the experimental results that Ni-related species in higher valence states could produce more CO. These findings establish new correlations between the catalytic performance and structural properties of Ni-based catalysts and provide catalyst synthetic strategies for controlling the metal oxidation state to achieve the selectivity in CO_2 hydrogenation reactions.

This work was supported by the U.S. Department of Energy (DOE, DE-SC0012704 and DE-AC02-05CH11231). Baohuai Zhao acknowledges the financial support from the China Scholarship Council (201606210159).

Notes and references

1 S. Choi, B. I. Sang, J. Hong, K. J. Yoon, J. W. Son, J. H. Lee, B. K. Kim and H. Kim, Sci. Rep., 2017, 7, 41207-41216.
2 M. D. Porosoff, B. Yan and J. G. Chen, *Energy Environ. Sci.*, 2016, **9**, 62-73.
3 F. Wang, S. He, H. Chen, B. Wang, L. Zheng, M. Wei, D. G. Evans and X. Duan, *J. Am. Chem. Soc.*, 2016, **138**, 6298-6305.
4 W. Lin, K. M. Stocker and G. C. Schatz, *J. Am. Chem. Soc.*, 2017, **139**, 4663-4666.
5 R. Zhou, N. Rui, Z. Fan and C.-j. Liu, *Int. J. Hydrogen Energ.*, 2016, **41**, 22017-22025.
6 W. Wang, S. Wang, X. Ma and J. Gong, *Chem. Soc. Rev.*, 2011, **40**, 3703-3727.
7 S. Kattel, W. Yu, X. Yang, B. Yan, Y. Huang, W. Wan, P. Liu and J. G. Chen, *Angew. Chem. Int. Ed. Engl.*, 2016, **55**, 7968-7973.
8 M. D. Porosoff and J. G. Chen, *J. Catal.*, 2013, **301**, 30-37.
9 Y. Liu and D. Liu, *Int. J. Hydrogen Energ.*, 1999, **24**, 351-354.
10 H. C. Wu, Y. C. Chang, J. H. Wu, J. H. Lin, I. K. Lin and C. S. Chen, *Catal. Sci. Technol.*, 2015, **5**, 4154-4163.
11 T. K. Campbell and J. L. Falconer, *Appl. Catal.*, 1989, **50**, 189-198.
12 S. Kattel, B. Yan, J. G. Chen and P. Liu, *J. Catal.*, 2016, **343**, 115-126.
13 S. Kattel, B. Yan, Y. Yang, J. G. Chen and P. Liu, *J. Am. Chem. Soc.*, 2016, **138**, 12440-12450.
14 S. Kattel, P. Liu and J. G. Chen, *J. Am. Chem. Soc.*, 2017, **139**, 9739-9754.
15 C. Heine, B. A. Lechner, H. Bluhm and M. Salmeron, *J. Am. Chem. Soc.*, 2016, **138**, 13246-13252.
16 R. V. Gonçalves, L. L. R. Vono, R. Wojcieszak, C. S. B. Dias, H. Wender, E. Teixeira-Neto and L. M. Rossi, *Appl. Catal. B: Environ.*, 2017, **209**, 240-246.
17 B. Mutz, H. W. P. Carvalho, S. Mangold, W. Kleist and J.-D. Grunwaldt, *J. Catal.*, 2015, **327**, 48-53.
18 D. Neagu, T. S. Oh, D. N. Miller, H. Menard, S. M. Bukhari, S. R. Gamble, R. J. Gorte, J. M. Vohs and J. T. Irvine, *Nat. Commun.*, 2015, **6**, 8120.
19 J. Deng, M. Cai, W. Sun, X. Liao, W. Chu and X. S. Zhao, *ChemSusChem*, 2013, **6**, 2061-2065.
20 R. Thalinger, M. Gocyla, M. Heggen, R. Dunin-Borkowski, M. Grünbacher, M. Stöger-Pollach, D. Schmidmair, B. Klötzer and S. Penner, *J. Catal.*, 2016, **337**, 26-35.
21 P. Steiger, R. Delmelle, D. Foppiano, L. Holzer, A. Heel, M. Nachtegaal, O. Krocher and D. Ferri, *ChemSusChem*, 2017, **10**, 2505-2517.
22 X. Liu, X. Liu, J. Meng, C. Yao, X. Zhang, J. Wang and J. Meng, *Int. J. Hydrogen Energ.*, 2016, **41**, 22361-22372.
23 M. Burriel, S. Wilkins, J. P. Hill, M. A. Muñoz-Márquez, H. H. Brongersma, J. A. Kilner, M. P. Ryan and S. J. Skinner, *Energy Environ. Sci.*, 2014, **7**, 311-316.
24 L. Qiao and X. Bi, *EPL (Europhysics Letters)*, 2011, **93**, 57002.
25 A. M. Tarditi, N. Barroso, A. E. Galetti, L. A. Arrúa, L. Cornaglia and M. C. Abello, *Surf. Interface Anal.*, 2014, **46**, 521-529.
26 L. Pino, A. Vita, M. Laganà and V. Recupero, *Appl. Catal. B: Environ.*, 2014, **148-149**, 91-105.
27 T. Avanesian and P. Christopher, *ACS Catal.*, 2016, **6**, 5268-5272.
28 T. Avanesian, G. S. Gusmão and P. Christopher, *J. Catal.*, 2016, **343**, 86-96.

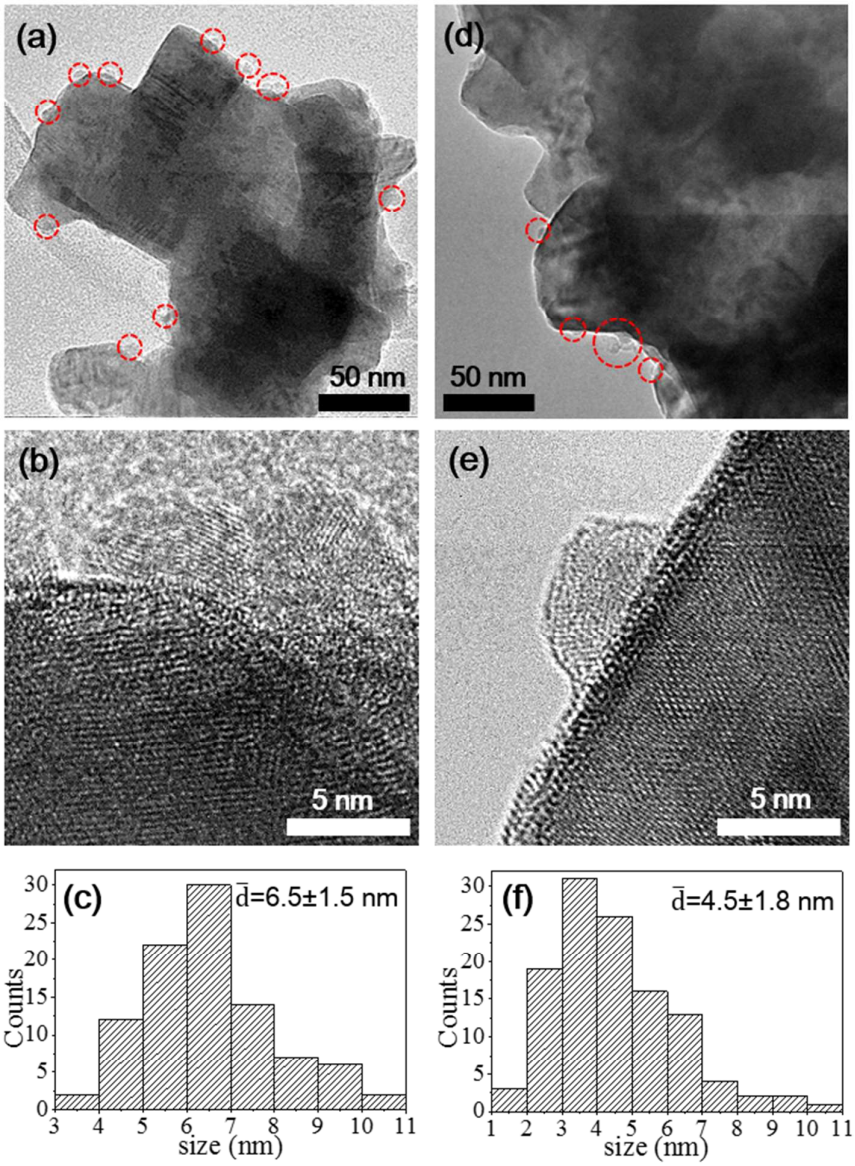

Fig. 1 TEM images and particle size distributions of the spent catalysts (a–c) $LaNiO_3$; (d–f) $LaFe_{0.5}Ni_{0.5}O_3$.

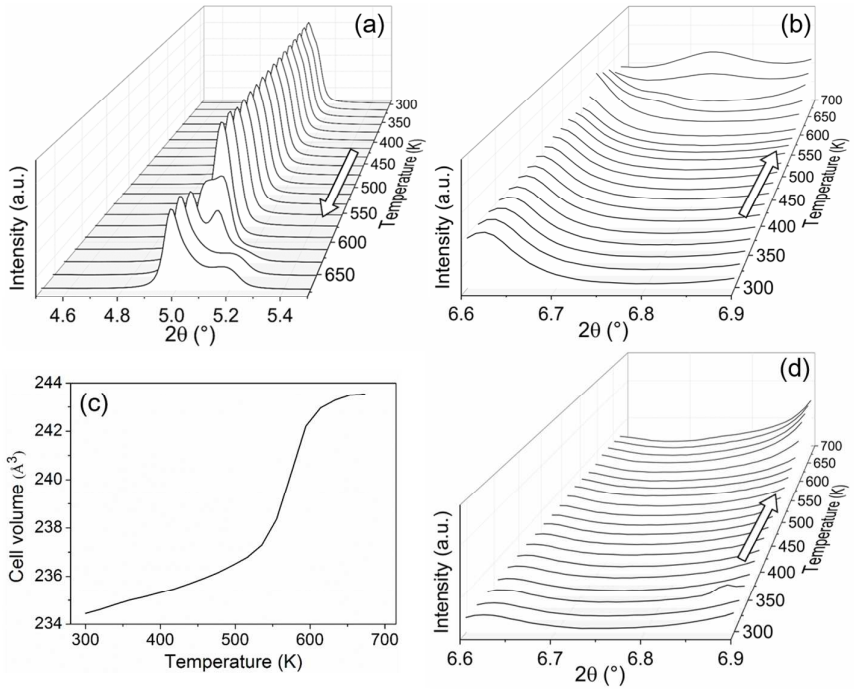

Fig. 2 Results of the *in-situ* XRD measurements during the temperature ramping stage, (a) and (b) patterns of $LaNiO_3$; (c) and (d) lattice expansion and patterns of $LaFe_{0.5}Ni_{0.5}O_3$. Fig. b and d show regions where Ni diffraction peaks would be expected.

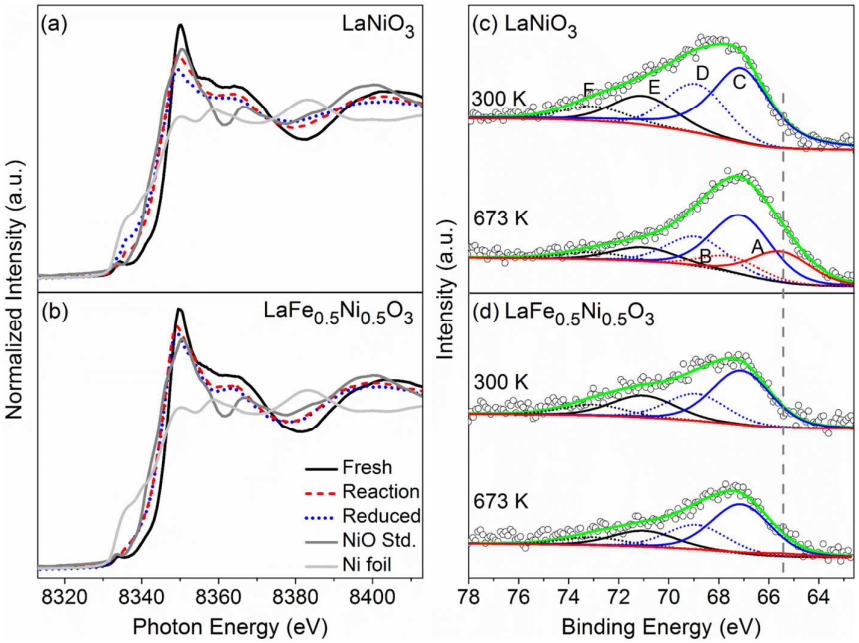

Fig. 3 *In-situ* XANES spectra of Ni K-edge of (a) $LaNiO_3$ and (b) $LaFe_{0.5}Ni_{0.5}O_3$. *In-situ* AP-XPS spectra of Ni 3*p* of (c) $LaNiO_3$ and (d) $LaFe_{0.5}Ni_{0.5}O_3$ at 300 K and 673 K, peak A and B correspond to the $3p_{3/2}$ and $3p_{1/2}$ of Ni^0, peak C and D correspond to the $3p_{3/2}$ and $3p_{1/2}$ of Ni^{2+}, peak E and F correspond to the $3p_{3/2}$ and $3p_{1/2}$ of Ni^{3+}.

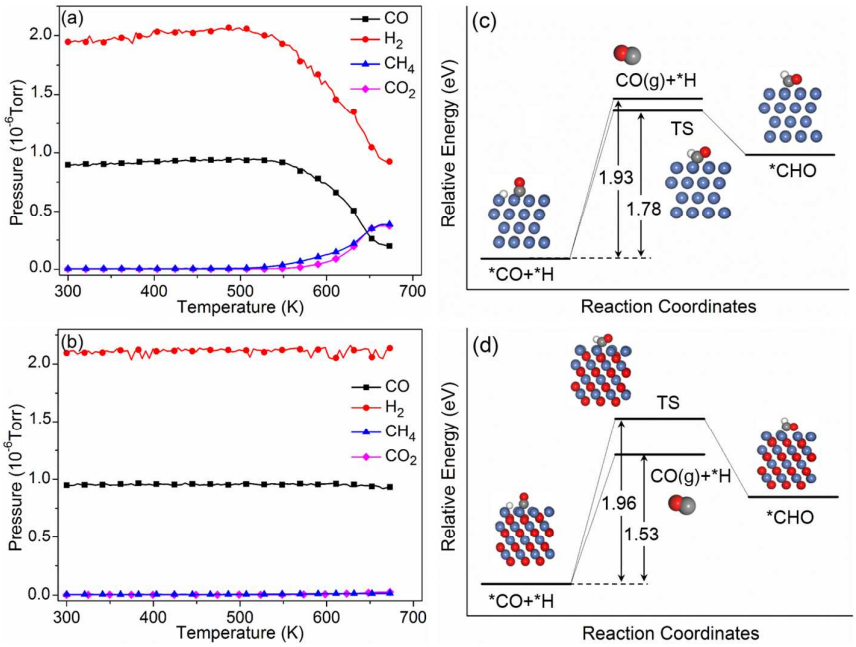

Fig. 4 The partial pressures of CO, H_2, CH_4, and CO_2 during the CO hydrogenation reaction for (a) $LaNiO_3$ and (b) $LaFe_{0.5}Ni_{0.5}O_3$. Potential energy diagram for the reaction routes of *CO+H on Ni(111) and NiO(111). The DFT optimized geometries of *H, *CO, transition states (TS), and *CHO on Ni(111) and NiO(111), are shown as insets in (c) and (d), Ni: blue, O: red, C: gray, H: white.

Table of contents entry

The product selectivity of CO_2 hydrogenation can be significantly tuned by controlling the valence state of Ni using perovskites.